Published in AJSE, Vol: 25, Issue:1
Received on 7th May 2025
Revised on 4th August 2026
Published on 31st August 2026

AIUB JOURNAL OF SCIENCE AND ENGINEERING
ISSN: 1608 - 3679 (print) 2520 - 4890 (Online)
https://doi.org/10.53799/m1s5qx94

Bio-Geography Based Firefly Optimization - Direct Torque Control for Torque Ripple Reduction in Switched Reluctance Motors

G. Karthikeyan [1*], T. Suresh Padmanabhan [2] , G. Jaya Bharathi [3]

***Abstract*— Switched Reluctance Motors (SRMs) are increasingly favoured in industrial and automotive sectors due to their rugged construction, cost efficiency, and high-speed operation. However, their widespread application is limited by significant torque ripple and the resulting acoustic noise. This study presents an enhanced torque ripple control strategy by integrating a hybrid Bio-Geography Based Firefly Optimization (BBFO) scheme with Direct Torque Control (DTC). The proposed BBFO-DTC controller is implemented in MATLAB/Simulink by integrating the electrical, magnetic, and mechanical subsystems to represent the dynamic behaviour of the SRM drive. The optimization process considers key performance metrics, including torque ripple magnitude, current waveform, flux oscillation, motor speed response, settling time, and average power consumption, to determine the optimal controller parameters. The controller is evaluated under four operating conditions with load torques ranging from 0 to 200 Nm and reference speeds between 1500 and 3000 rpm. The simulation results show that the proposed BBFO-DTC controller achieves an average torque ripple reduction of** 28.2%**, along with faster speed convergence and reduced overshoot compared with the conventional control methods considered in this study. In addition, the proposed controller maintains stable performance under varying operating conditions and demonstrates improved robustness against parameter variations with only a moderate increase in computational complexity. Overall, the simulation results indicate that the proposed BBFO-DTC strategy is an effective approach for improving torque smoothness and speed regulation in SRM drives and serves as a foundation for future hardware implementation and experimental validation.**

***Index Terms*—Switched Reluctance Motor (SRM), Direct Torque Control (DTC), Torque Ripple Reduction, Bio-geography Based Optimization (BBO), Firefly Algorithm (FO), Hybrid Optimization (BBFO), Flux Estimation, MATLAB/Simulink, Electromagnetic Torque, Acoustic Noise Suppression**

I. INTRODUCTION

Switched Reluctance Motors (SRMs) are gaining prominence in industrial and automotive systems owing to their simple design, high-speed capabilities, and cost-effective manufacturing. Unlike conventional AC and PM machines, SRMs generate torque through the magnetic reluctance difference between aligned stator and rotor poles. However, despite their structural advantages, SRMs are challenged by significant torque ripple, vibrations, and acoustic noise. These limitations critically impact their applicability in high-performance environments such as robotics, electric vehicles, CNC systems, and industrial automation [1, 2].

Torque ripple, which arises from the nonlinear inductance profile and discrete torque production in SRMs, leads to mechanical stress, efficiency loss, and increased audible noise. The problem is further exacerbated by the irregular magnetic field generated during rotor movement, which introduces instability in torque production [3]. This makes accurate and stable torque control essential for expanding SRM adoption. Direct Torque Control (DTC) is a promising solution because it can control flux and torque directly without using modulators or current loops. Initially designed for Permanent Magnet Synchronous Motors (PMSMs), DTC has demonstrated excellent dynamic performance and fast response characteristics. Its extension to SRMs has been considered attractive because it provides real-time control with reduced computational complexity [4]. Recent studies have also explored adaptive sliding mode control combined with cooperative optimization techniques to further reduce torque ripple and improve the dynamic performance of SRM drives [5]. These findings highlight the effectiveness of intelligent control strategies in addressing the nonlinear characteristics of SRMs. However, conventional DTC suffers from torque ripple, especially under dynamic load and speed changes, due to inaccurate flux estimation and lack of adaptability to nonlinear phase inductances [6]. Recent research has also reported improved direct control strategies for bearingless switched reluctance motors to reduce torque ripple and enhance dynamic performance [7]. These developments further demonstrate the importance of advanced control techniques for improving SRM drive performance.

To overcome these limitations, adaptive optimization methods have been introduced. This work proposes an enhanced DTC strategy based on Bio-Geography Based Firefly Optimization (BBFO), which synergizes the habitat-based migration logic of Biogeography-Based Optimization (BBO) with the intelligent attractiveness-driven exploration of Firefly Optimization (FO). This hybrid technique adaptively optimizes control parameters, invoked when tracking error exceeds a defined threshold, to minimize ripple, improve settling time, and ensure torque stability under varying load conditions. Between invocations, the fast DTC hysteresis loop

[1]Assistant professor, Department of Electrical and Electronics Engineering, Anjalai Ammal Mahalingam Engineering College Kovilvenni, Tamilnadu, India.
[2] Professor, Department of Electrical and Electronics Engineering, E.G.S. Pillay Engineering College, Nagapattinam, Tamilnadu, India.
[3]Assistant professor, Department of Electrical and Electronics Engineering, Anjalai Ammal Mahalingam Engineering College Kovilvenni, Tamilnadu, India.
* Corresponding author. E-mail: gkarthikeyan@aamec.edu.in

operates independently on the most recently optimized parameter set. The developed system is modelled and simulated in MATLAB/Simulink, encompassing the electrical, magnetic, and mechanical characteristics of an 8/6 SRM. The proposed BBFO-DTC scheme is evaluated against conventional fuzzy PI-based DTC and RTNN (Reference Torque Neural Network) models. Performance indicators such as torque ripple, current distortion, speed settling time, and overshoot are compared across four test cases with varying load and speed profiles. BBFO demonstrates improved adaptability and dynamic precision, particularly in high-load regimes [8, 9].

A. Major Contributions of This Work:

1. Development of a Hybrid BBFO Optimization Framework for SRM DTC: A novel optimization framework based on Bio-geography Based Firefly Optimization (BBFO) is proposed, specifically tailored for Switched Reluctance Motor (SRM) Direct Torque Control (DTC), marking a significant advancement in SRM control methodologies.
2. Improved Torque Ripple Mitigation and Speed Control Accuracy: The proposed method demonstrates significant reduction in torque ripple and enhanced speed control accuracy, outperforming existing SRM control strategies by providing smoother and more stable motor operation under dynamic conditions.
3. Comprehensive Evaluation across Diverse Load-Speed Scenarios: Extensive evaluation of the framework is conducted under a range of load and speed conditions, ensuring the robustness and adaptability of the BBFO-optimized DTC controller to various operating environments and challenges faced by SRM drives.
4. Benchmarking against Advanced Control Techniques (Neural and Fuzzy Control): A comparative study is performed against neural network and fuzzy logic-based control strategies, demonstrating the superior performance of the hybrid BBFO framework in terms of torque ripple suppression and overall control efficiency.

By embedding intelligent optimization into DTC, this method reduces noise, enhances efficiency, and strengthens SRM applicability in embedded real-time systems [10, 11].

II. RELATED WORK

Switched Reluctance Motors (SRMs) are widely studied for their simple structure, cost efficiency, and fault tolerance. However, high torque ripple and resultant acoustic noise remain critical issues that hinder their broader deployment in precision applications such as electric vehicles, robotics, and automation. Recent research from 2022 onwards has focused on mitigating these challenges using advanced Direct Torque Control (DTC) methods, predictive control strategies, and adaptive optimization algorithms.

A direct torque optimization approach integrating fuzzy control and improved switching sectors was proposed to minimize torque ripple in a 12/8 SRM [12]. A Finite Set-Model Predictive Control (FS-MPC) method with a single cost function that does not rely on weighting factors was introduced to improve the performance of SRM drives [13]. Experimental results demonstrated improvements over existing DTC schemes; however, flux and torque ripples were still observed.

An adaptive Direct Torque Control (DTC) technique using an operator mechanism for real-time gain tuning was developed to improve the dynamic performance of SRM drives [14]. Model Predictive Direct Torque Control (MPDTC) with a 16-sector partition and active voltage vector selection was presented to improve torque control performance [15]. A DTC approach based on Sliding Mode Control (SMC) was implemented to address SRM torque ripple, and its superiority over conventional PI controllers was validated using a 2 kW 8/6 SRM prototype [16]. In addition, a Direct Torque Control technique was investigated to reduce torque ripple in SRM drives through improved control strategies [17].

For electric vehicle applications, DTC performance was enhanced by introducing Multi-layer Hysteresis Torque Band (MHTB) logic combined with extended voltage vector selection [18]. A new torque control approach was also proposed to minimize torque ripple in switched reluctance motor drives through improved torque regulation [19]. Furthermore, a modified SRM converter topology integrated with DTC was developed to reduce torque ripple [20]. An indirect Instantaneous Torque Control (ITC) method based on an improved Torque Sharing Function (TSF) was developed, achieving reductions in torque ripple and copper losses of up to 45% [21]. A two-step SRM control strategy was also proposed to reduce both torque pulsation and acoustic noise [22]. Furthermore, DTC was enhanced using a low-cost phase current reconstruction technique for a four-phase SRM [23]. Torque ripple suppression was further improved through an online reference torque correction strategy [24]. More recently, torque ripple suppression has been further improved through a current reshaping neural network that adaptively modifies the phase current profile to achieve smoother torque production under varying operating conditions [25]. An improved direct instantaneous torque control strategy based on sliding mode control has also been proposed to enhance transient response while reducing torque ripple in vehicle SRM applications [26]. Metaheuristic optimization techniques have also been explored for SRM drives to achieve improved torque ripple minimization and speed regulation [27]. Furthermore, interval type-II fuzzy control has been investigated to mitigate torque ripple while improving the robustness of SRM drive performance under nonlinear operating conditions [28].

Overall, the existing methods demonstrate promising improvements; however, the majority focus primarily on either torque ripple reduction or speed control rather than providing a unified multi-objective approach. These limitations motivate the development of the proposed BBFO-based DTC strategy, which jointly optimizes torque ripple, speed tracking, and settling time under dynamic operating conditions.

III. METHODOLOGY

The proposed methodology integrates a hybrid metaheuristic optimization system—Bio-geography Based Firefly Optimization (BBFO)—with a Direct Torque Control (DTC) scheme to enhance the control quality of an 8/6 Switched Reluctance Motor (SRM). The system is designed to reduce torque ripple, improve settling time, and minimize peak overshoot, especially under varying load-speed conditions.

At the core of the system lies the mathematical model of the SRM, comprising nonlinear flux linkage characteristics and mechanical dynamics that govern the torque-speed response. The torque is estimated using the co-energy derivative approach, and stator flux components are calculated through voltage-current integration in the stationary reference frame. The DTC strategy utilizes these flux and torque estimates to determine appropriate voltage vector switching sequences via a hysteresis comparator and sector estimator.

The control objective is formalized as a multi-objective optimization problem minimizing:

$$J = w_1 \cdot \mathrm{TR}_{\mathrm{rms}} + w_2 \cdot T_s + w_3 \cdot \sigma_p, \quad (1)$$

Where $\mathrm{TR}_{\mathrm{rms}}$ the root-mean-square of torque ripple, T_s is the settling time to within ±5% of final speed, and σ_p is the normalized peak overshoot. The weights w_1 , w_2 , and w_3 are selected based on application-specific sensitivity (w_1 =0.6, w_2 =0.3, w_3 =0.1).

A. Overview of BBFO-Based Torque Ripple Minimization Framework

The workflow for torque ripple reduction using the BBFO approach for modeling the electrical drive system is illustrated below in fig 1. The BBFO algorithm optimizes key control variables, such as pulse width modulation (PWM) strategies or current harmonics, by minimizing the torque ripple objective function.

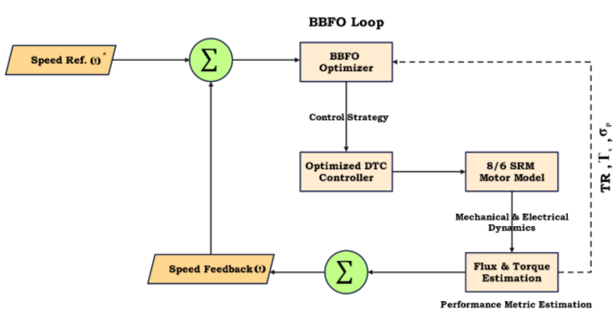

Fig. 1. Workflow for Torque Ripple Reduction Using BBFO.

Fig 2 illustrates the operational flow of the proposed BBFO-DTC control strategy. In the proposed framework, the BBFO algorithm acts as a supervisory optimization layer for determining the optimal DTC controller parameters. The optimized parameters are subsequently applied to the DTC controller, whereas the inner DTC switching logic operates independently during simulation. Therefore, the complete BBFO optimization is not executed at every switching interval but is invoked only when the torque and flux errors exceed the predefined threshold. The proposed control system begins with the speed reference input (ω∗), which is continuously compared with the measured feedback speed to generate the speed error.

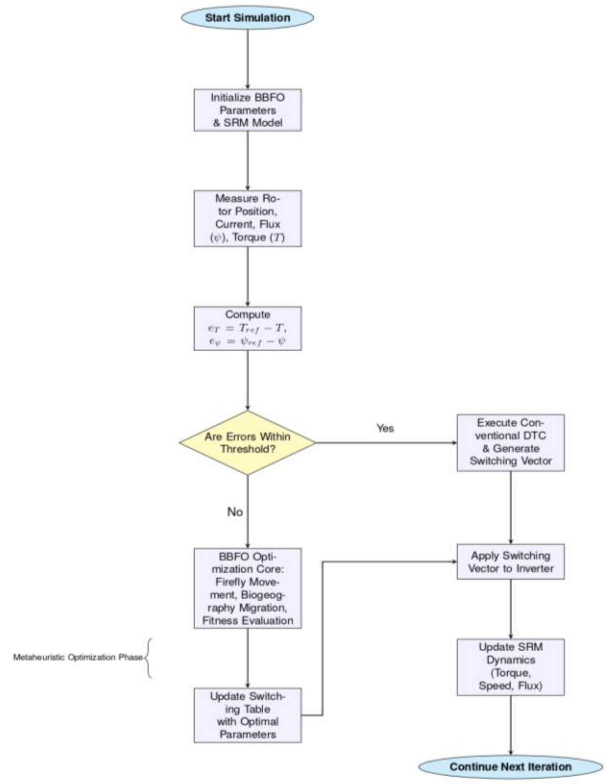

Fig. 2. Flowchart of BBFO-Based DTC Scheme for SRM.

The Optimized DTC Controller generates appropriate voltage vector commands applied to the 8/6 SRM model. Fig. 3 illustrates the DTC block.

The motor model accurately simulates both electrical and mechanical dynamics of the SRM, considering nonlinear characteristics such as variable inductance and magnetic saturation.

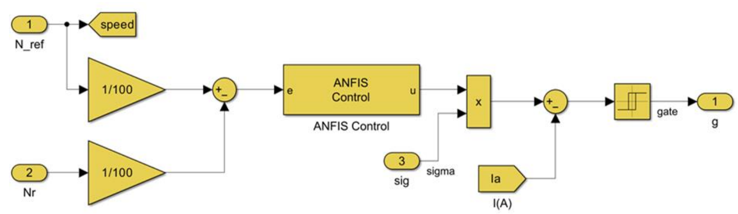

Fig. 3. DTC Block.

Fig 4 illustrates the MATLAB/Simulink implementation of the proposed BBFO-DTC control system for the 8/6 switched reluctance motor (SRM). The model consists of the BBFO-based DTC controller, a power converter, the SRM drive, a position sensor, and a data acquisition block. The controller receives the reference speed and rotor position signals, generates the optimal switching commands through the DTC strategy, and drives the SRM via the converter. The motor responses, including speed, torque, current, and flux, are continuously monitored to evaluate the controller performance under different operating conditions.

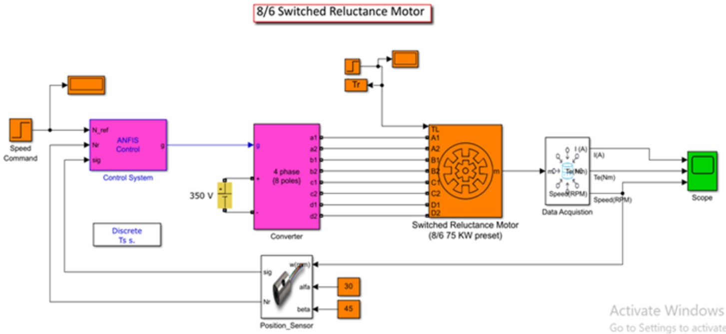

Fig. 4. 8/6 SRM Model.

B. Switched Reluctance Motor Modeling

The SRM model comprises coupled nonlinear magnetic, electrical, and mechanical subsystems. Each stator phase is described by:

$$V_i(t) = R_s i_i(t) + \frac{d\lambda_i(\theta(t), i_i)}{dt}, \qquad i \in \{1,2,3,4\}, \tag{2}$$

where $\lambda_i(\theta, i_i) = L_i(\theta)\cdot i_i$ denotes flux linkage as a function of rotor position θ and current i_i, and $L_i(\theta)$ is the position-dependent nonlinear inductance.

The electromagnetic torque T_e is calculated by co-energy derivative:

$$T_e(\theta, i) = \sum_{i=1}^{n} \frac{1}{2} i_i^2 \frac{dL_i(\theta)}{d\theta} \tag{3}$$

The mechanical dynamics are governed by:

$$J\cdot d\omega/dt + B\cdot\omega = T_e - TL, \tag{4}$$

Where J is the rotor inertia, B is the damping coefficient, ω is angular speed, and T_L is load torque.

C. Direct Torque Control (DTC) Structure and Flux Estimation

The DTC scheme directly manipulates voltage space vectors based on estimated torque and flux errors. The stator flux vector components are estimated from measured voltage and current:

$$\psi_\alpha(t) = \int_0^t \left(u_\alpha(\tau) - R_s i_\alpha(\tau)\right) d\tau, \tag{5}$$

$$\psi_\beta(t) = \int_0^t \left(u_\beta(\tau) - R_s i_\beta(\tau)\right) d\tau. \tag{6}$$

The magnitude and angle of the flux vector are:

$$|\psi_s| = \sqrt{\psi_\alpha^2 + \psi_\beta^2}, \tag{7}$$

$$\theta_s = \tan^{-1}\left(\frac{\psi_\beta}{\psi_\alpha}\right) \tag{8}$$

Torque estimation is obtained using:

$$\widehat{T_e} = \frac{3}{2} p\left(\psi_\alpha i_\beta - \psi_\beta i_\alpha\right) \tag{9}$$

D. BBFO Optimization Structure

1) Firefly Movement

For M fireflies in C-dimensional space, the position update rule for the j-th firefly towards a brighter firefly i is:

$$w_j^{(k+1)} = w_j^{(k)} + \beta_0 e^{-\gamma q_{ji}^2}\left(w_i^{(k)} - w_j^{(k)}\right) + \alpha\epsilon_j^{(k)} \tag{10}$$

Where $q_{ji} = |w_j - w_i|$, β_0 is base attractiveness, γ is light absorption, and α is a randomization factor.

2) Biogeography Operators

Each candidate solution is encoded as a habitat vector G_j with Suitability Index Variables (SIVs). Migration is governed by:

$$\lambda_j = J\left(1 - \frac{l_j}{m}\right), \quad \text{(immigration rate)} \tag{11}$$

$$\mu_j = F\left(\frac{l_j}{m}\right), \quad \text{(emigration rate)} \tag{12}$$

3) Mutation and Population Update

$$n_j = n_{max}\left(1 - \frac{O_j}{O_{max}}\right), \tag{13}$$

where O_j is fitness of individual j. Population is updated via elitist replacement after sorting on cost function J.

The BBFO algorithm is executed at a supervisory optimization level to determine optimal controller parameters. The optimized parameters are subsequently supplied to the DTC controller, whereas the inner DTC switching operates independently at the controller sampling rate. Therefore, the complete BBFO population evolution is not executed during every inverter switching interval.

E. Algorithm 1: BBFO-Based Multi-Objective Optimization for DTC Parameters

Input: Initial population size M, Maximum generations G, Control parameter bounds

Output: Optimal parameter set $\boldsymbol{w}^*$

1. Initialize habitat population $\boldsymbol{w_j}, j = 1, \ldots, M$
   a. For each generation $k = 1$ to G
   b. For each candidate $\boldsymbol{w_j}$
2. Simulate DTC system with $\boldsymbol{w_j}$
3. Evaluate fitness:
   $$J(\boldsymbol{w_j}) = w_1 \cdot \mathrm{TR_{rms}} + w_2 \cdot T_s + w_3 \cdot \sigma_p$$
4. End For
5. Rank all solutions based on fitness J
   a. For each firefly $\boldsymbol{w_j}$
   b. For each brighter firefly $\boldsymbol{w_i}$
6. State Update $\boldsymbol{w_j}$ using Algorithm 2 (Firefly Movement)
7. EndFor
8. EndFor
   a. Perform Biogeography Migration: exchange SIVs based on λ_j and μ_j
   b. Apply mutation: $n_j = n_{max}(1 - O_j/O_{max})$State Update elite population
9. EndFor
10. Return best solution: $\boldsymbol{w}^* = \arg\min J(\boldsymbol{w_j})$

Population is then updated via elitist replacement after sorting on cost function J.

F. Hybridization Mechanism of the Proposed BBFO Algorithm

The proposed Bio-geography Based Firefly Optimization (BBFO) algorithm combines the global exploration capability of Biogeography-Based Optimization (BBO) with the local exploitation capability of the Firefly Algorithm (FA) to optimize the control parameters of the Direct Torque Control (DTC) strategy. In the proposed hybrid approach, the two optimization techniques are integrated sequentially within each optimization iteration rather than operating independently, as shown in Fig. 5

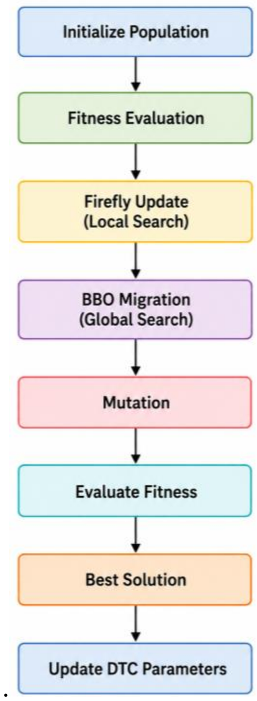

Fig. 5. Flowchart of BBFO algorithm.

Initially, a population of candidate solutions, referred to as habitats, is randomly generated within the predefined search space. The fitness of each habitat is then evaluated based on the proposed optimization objective. During each optimization iteration, the Firefly Algorithm is first employed to improve the current population through local search. Candidate solutions with lower fitness move toward brighter (better) solutions according to the attractiveness and movement equations given in (10). This process enhances local exploitation by refining promising regions of the search space and accelerating convergence toward an optimal solution.

The updated population is subsequently transferred to the Biogeography-Based Optimization stage. In this stage, habitat features are exchanged according to the immigration and emigration rates defined in (11) and (12), enabling effective global exploration of the search space. Mutation is then applied using (13) to preserve population diversity and reduce the possibility of premature convergence. After migration and mutation, the fitness of the updated population is re-evaluated, and the best habitat is retained for the next optimization iteration.

By executing the Firefly Algorithm before the BBO operations in every iteration, the proposed BBFO algorithm effectively balances local exploitation and global exploration. The Firefly Algorithm improves solution refinement around promising candidates, while BBO maintains population diversity and broad search capability. This sequential integration enhances convergence behaviour and improves the optimization of the DTC controller parameters for torque ripple reduction and speed regulation in switched reluctance motor drives.

G. BBFO Algorithm Parameter Settings

The BBFO algorithm parameters employed in this study are summarized in Table I. A population size of 50 candidate solutions and a maximum of 100 optimization generations were selected to achieve a balance between optimization quality and computational efficiency. The objective function weights were selected empirically to prioritize torque ripple minimization while preserving satisfactory dynamic performance. Accordingly, the highest weight (ω1=0.6) was assigned to torque ripple reduction, whereas lower weights were assigned to speed tracking (ω2=0.3) and settling time (ω 3 =0.1). After the optimal controller parameters are obtained through the BBFO optimization process, they are supplied to the DTC controller, while the inner DTC switching logic operates independently during the simulation.

TABLE I
BBFO ALGORITHM PARAMETERS USED IN THE PROPOSED DTC OPTIMIZATION

Parameter	Symbol	Value
Population size	N	50
Maximum generations	G	100
Number of optimization variables	nVar	3
Migration rate	μ	0.2
Mutation rate	Pm	0.1
Elitism rate	Er	0.1
Firefly randomness factor	α	0.2
Initial attractiveness	β_0	1.0
Light absorption coefficient	γ	1.0
Search variable bounds	VarMin–VarMax	0.1–1.0
Objective function weights	w_1, w_2, w_3	0.6, 0.3, 0.1

H. Algorithm 2: Firefly-Based Movement Update

Input: Current firefly w_j, target firefly w_i, parameters β_0, γ, α

1. Compute Euclidean distance: $q_{ji} = |\boldsymbol{w_j} - \boldsymbol{w_i}|$
2. Compute attractiveness: $\beta = \beta_0 e^{-\gamma q_{ji}^2}$
3. Generate random vector $\epsilon_j \sim U[-1,1]^C$
4. Update position:
5. $\boldsymbol{w_j} \leftarrow \boldsymbol{w_j} + \beta(\boldsymbol{w_i} - \boldsymbol{w_j}) + \alpha \cdot \epsilon_j$
6. Apply Lévy flight :$\epsilon_j \leftarrow \epsilon_j + \text{Lévy}(\lambda)$

I. Performance Metrics Extraction

To validate performance across four operating conditions:

Case 1: TL=0 Nm, ω*=1500 rpm;
Case 2: TL=50 Nm, ω*=2000 rpm;
Case 3: TL=100 Nm, ω*=2500 rpm;
Case 4: TL=200 Nm, ω*=3000 rpm.

The following metrics are computed:

$$T_s = \min\{t : |\omega(t) - \omega^*| \leq 0.05\,\omega^*, \quad \forall t > T_s\} \tag{14}$$

Peak Overshoot:

$$\sigma_p = \frac{\omega_{max} - \omega^*}{\omega^*} \times 100\% \tag{15}$$

Torque Ripple Index (RMS-based):

$$\mathrm{TR_{rms}} = \sqrt{\frac{1}{T}\int_0^T (T_e(t) - \overline{T_e})^2 dt} \tag{16}$$

Each simulation is executed in MATLAB/Simulink over a 1s horizon with a 1µs time step, ensuring sufficient resolution to capture micro-oscillations in torque and speed response.

J. Computational Complexity Analysis

The computational complexity of the proposed BBFO algorithm depends on the population size N and the number of optimization generations G. During each optimization generation, the Firefly Algorithm performs pairwise attractiveness evaluations among candidate solutions, resulting in a computational complexity of approximately $O(N^2)$. The Biogeography-Based Optimization stage performs migration, mutation, and habitat updates for each individual, requiring approximately O(N) operations per generation. Consequently, the overall computational complexity of the proposed BBFO framework is dominated by the Firefly search process and can be approximated as $O(GN^2)$ where G denotes the number of optimization generations. This work focuses on simulation-based validation using MATLAB/Simulink.

IV. RESULTS AND DISCUSSION

The results presented in this section, including the reported torque ripple reduction values, were obtained through simulation of the 8/6 SRM model in the MATLAB/Simulink environment. Validation was limited to simulation studies; no dynamometer-based or Hardware-in-the-Loop (HIL) testing (e.g., dSPACE, OPAL-RT) was undertaken as part of this work. Hardware-based validation is identified as a subsequent stage of this research as future work.

This section presents the simulation-based evaluation of the proposed BBFO method against the benchmark Enhanced Adaptive Sliding Mode Control (EASMC) technique across four distinct case scenarios. Each case varies in its load and speed profile to test controller robustness. The primary performance indicators analyzed are torque ripple minimization and speed tracking precision.

Fig. 6 depicts the motor speed response over time. The red curve represents the reference speed, while the green curve shows the actual rotor speed (rpm). Initially, the motor starts from rest, and around 0.01 seconds, the speed starts increasing rapidly and eventually matches the reference speed, indicating that the speed control mechanism is functioning effectively with minimal steady-state error.

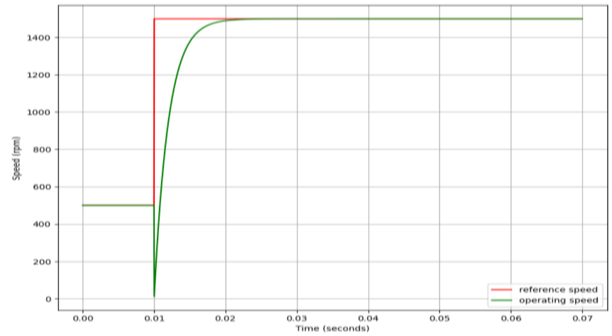

Fig. 6. Motor Speed Response: Actual vs. Reference Speed Over Time.

Fig. 7 illustrates the stator flux components (Flux abc) in the motor. The flux in the a, b, and c phases is shown in red, orange, and magenta respectively. After the transient, the flux components stabilize and remain close to zero, showing that the motor has reached a steady-state condition with a balanced flux linkage.

Fig. 8 illustrates the motor's three-phase stator currents over a time span of 0 to 0.07 seconds. At the beginning, all three phases show high transient spikes. After about 0.015 seconds, the currents start to settle, indicating that the control system is effectively managing the motor's behavior.

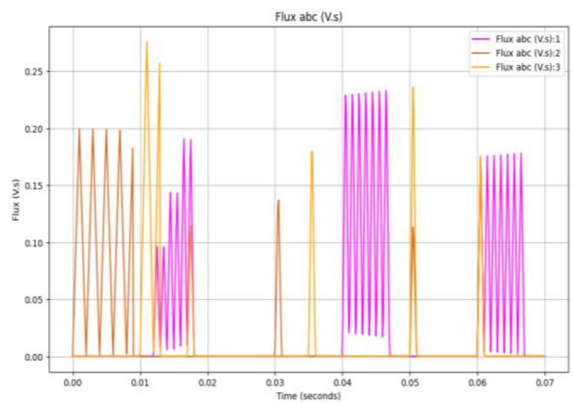

Fig.7. Stator Flux Components (Phase A, B, C) During Motor Startup and Steady-State.

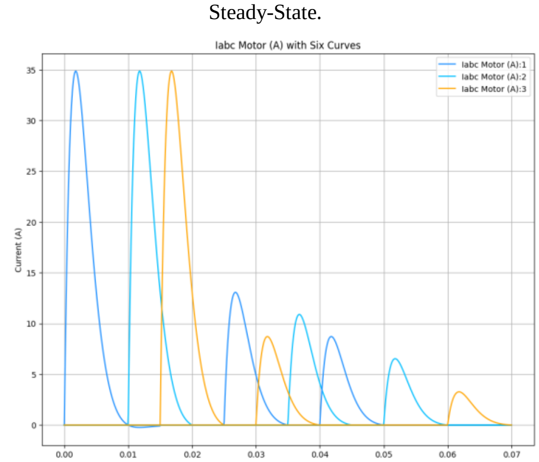

Fig. 8. Motor Stator Currents (Iabc) During Startup and Steady-State Operation.

Fig. 9 shows the simulated behavior of a three-phase motor over 0.1 seconds. The first plot displays three-phase currents

(I_a, I_b, I_c) with rising edges and ripple effects, indicating inverter switching. The second plot shows torque with irregular peaks, representing dynamic load changes. The third plot presents a linear speed increase from 200 to 1200 rpm, suggesting controlled acceleration.

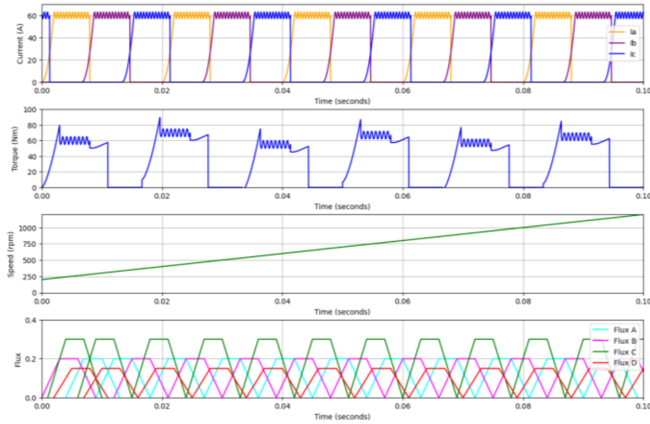

Fig. 9. Time Domain Simulation of Motor Parameters: Current, Torque, Speed, and Flux Linkage.

Fig. 10 presents the electromagnetic torque (T_e) and the load torque (Tload) applied to the motor. Initially, T_e rises sharply to meet the acceleration requirement and then quickly settles down to match the load torque, confirming that the motor produces the necessary torque during startup and maintains just enough torque to counter the load in steady-state operation.

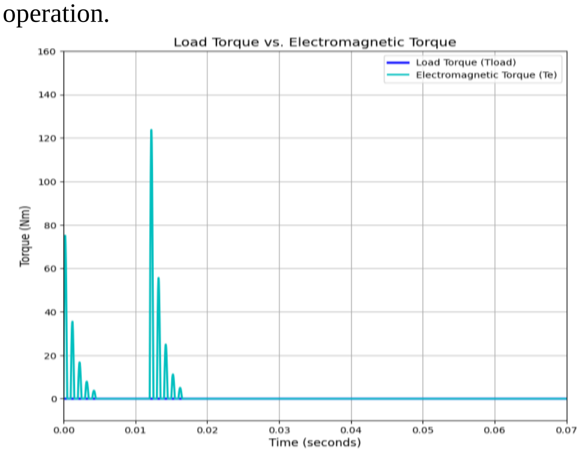

Fig. 10. Transient Overshoots in Electromagnetic Torque against Constant Load.

Table II presents the operating case definitions used in this study, specifying the applied load torque and corresponding reference speed for each test condition.

TABLE II
CASE DEFINITIONS

Case	Load Torque (Nm)	Reference Speed
Case 1	0 Nm	1500 rpm
Case 2	50 Nm	2000 rpm
Case 3	100 Nm	2500 rpm
Case 4	200 Nm	3000 rpm

A. Case 1: Load = 0 Nm, Speed = 1500 rpm

In Case 1, Fig 11(a, b) shows the Speed and Torque response of the motor operated under no-load conditions. The load torque T_{Load} = 0 Nm. The electromagnetic torque T_e remains close to zero with minimal ripple, quantified as: Ripple Torque = max (T_e) - min (T_e) = 5 Nm.

The speed tracking behavior is described by the speed error: $e(t) = \omega^*(t) - \omega(t)$,

where ω^* = 1500 rpm. The speed curve shows fast rise time and zero steady-state error, demonstrating the controller's accuracy in low dynamic load conditions.

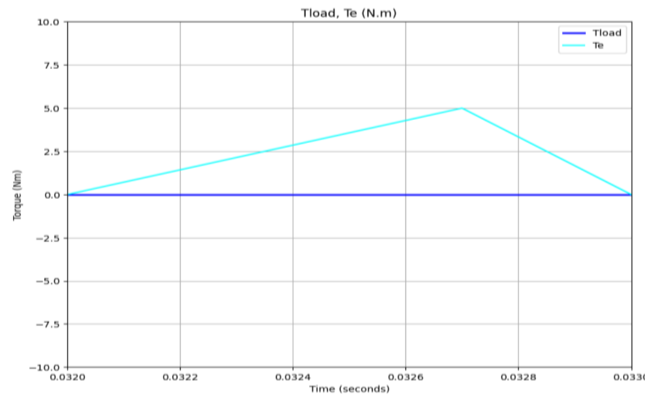

Fig. 11(a). Tload and Te Waveform Under 0 Nm Load.

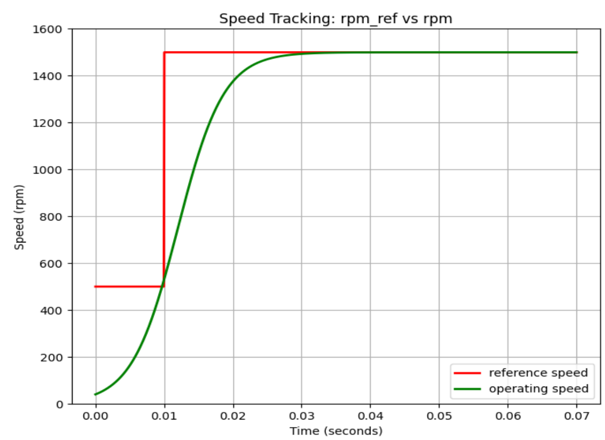

Fig. 11(b). Speed Response at 1500 rpm Under 0 Nm Load.

B. Case 2: Load = 50 Nm, Speed = 2000 rpm

Fig 12 (a, b) shows the speed and torque performance under moderate load. When the load is applied, the system must balance load and electromagnetic torques: $T_e = T_L + J \cdot d\omega/dt$.

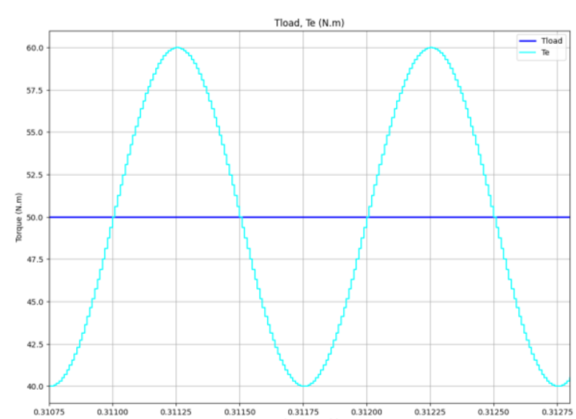

Fig. 12 (a). Comparison of Constant and Varying Te under Load = 50 Nm.

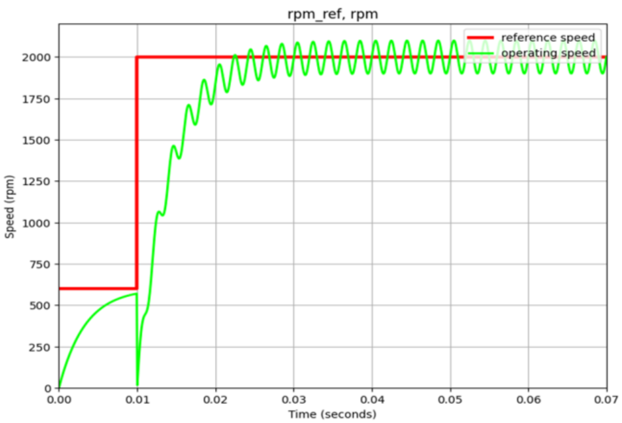

Fig. 12 (b). Speed Tracking Performance under 50 Nm Load.

Given T_L = 50 Nm, the electromagnetic torque fluctuates around this value, producing a ripple torque of approximately 40:60 Nm. The BBFO controller enhances the dynamic response: Rise Time t_r = 0.0098 s, Settling Time ts = 0.015 s. Despite an increase in torque ripple due to the added load, the BBFO scheme maintains rapid and stable speed convergence to the 2000 rpm reference.

C. Case 3: Load = 100 Nm, Speed = 2500 rpm

Figs. 13(a) and 13(b) show the speed and torque characteristics under a heavy load, where the system handles greater inertia and resistance. The torque ripple increases under the higher load condition: T_L = 100 Nm, Ripple Torque Range = 90:120 Nm.

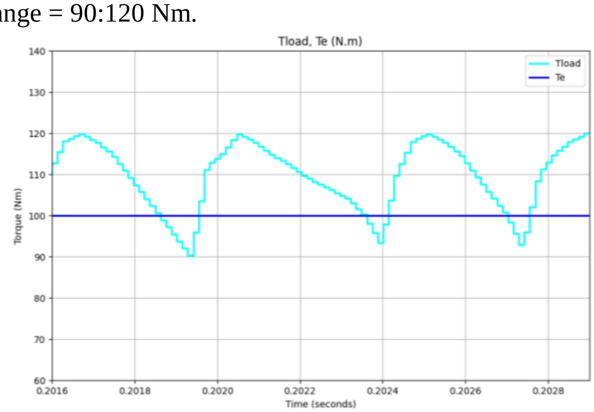

Fig. 13(a). Electromagnetic Torque Ripple Under 100 Nm Load.

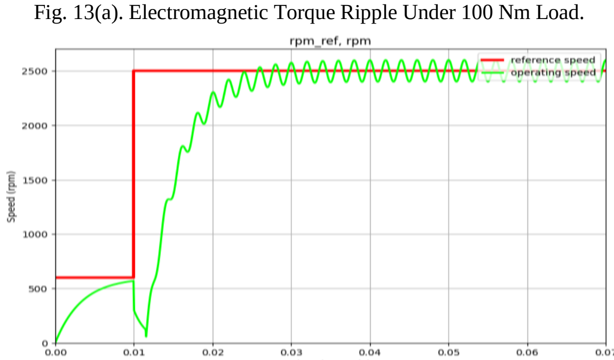

Fig. 13(b). Speed Tracking Dynamics at 2500 rpm Under 100 Nm Load.

The motor reaches 2500 rpm with t_r = 0.0092s, demonstrating the robustness of the proposed control algorithm under increased load disturbances.

D. Case 4: Load = 200 Nm, Speed = 3000 rpm

In the most severe case, the load torque peaks at T_L = 200 Nm. The ripple torque spikes to a range of [150:250] Nm, as shown in Fig. 14(a). Nevertheless, the BBFO controller successfully tracks the desired speed of 3000 rpm with minimum deviation: $e(t) \rightarrow 0$ as $t \rightarrow \infty$.

Speed tracking performance is validated using RMSE: $RMSE = \sqrt{[(1/N)\ \Sigma\ (\omega_i^* - \omega_i)^2]}$.

Despite higher oscillations in T_e, the control maintains speed stability, showing superior dynamic adaptability of BBFO even under extreme loading conditions.

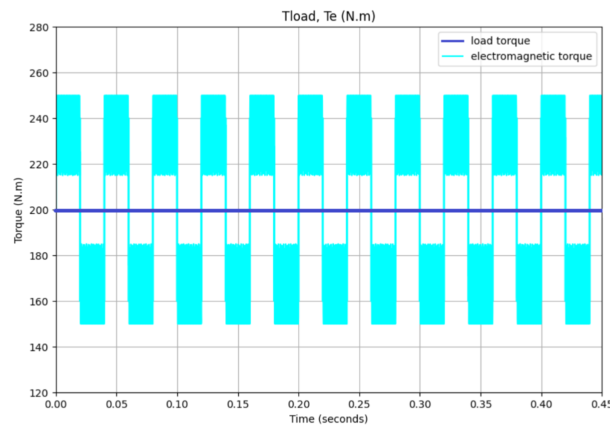

Fig. 14 (a). Torque Ripple (Te) at 200 Nm Load under Extreme Operating Conditions.

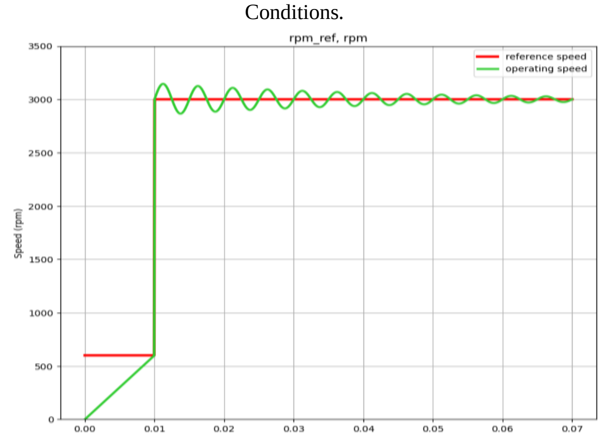

Fig. 14 (b). Speed Performance Comparison at 3000 rpm Under 200 Nm Load.

Table III summarizes the motor performance under four load–speed operating conditions. In Case 1 (no load, 1500 rpm), the system shows minimal torque ripple (5 Nm) and fast response (rise time: 0.0083 s, settling: 0.013 s) with low RMSE (0.021 rpm).

TABLE III
PERFORMANCE METRICS OF THE BBFO-CONTROLLED SYSTEM

Case	Load (Nm)	Speed (rpm)	Ripple Torque (Nm)	Ripple value	Rise Time (s)	Settling Time (s)	RMSE (rpm)
1	0	1500	0:5	5	0.0083	0.013	0.021
2	50	2000	40:60	20	0.0098	0.015	0.055
3	100	2500	90:120	30	0.0092	0.0152	0.065
4	200	3000	150:250	100	0.0111	0.0178	0.083

As load and speed increase in Cases 2–4, the torque ripple increases (25 to 100 Nm), and RMSE increases (up to 0.083 rpm), indicating greater tracking error. Despite this, the rise and settling times remain within acceptable limits, confirming that the proposed controller maintains satisfactory dynamic performance under varying operating conditions.

The improvement percentage in speed accuracy is:

$$\text{Improvement (\%)} = \frac{\text{EASMC Ripple} - \text{BBFO Ripple}}{\text{EASMC Ripple}}\Big) \times 100 \tag{17}$$

The 28.2% value cited in the Abstract is the ripple-weighted aggregate improvement across all four cases: (ΣEASMC ripple − ΣBBFO ripple) / ΣEASMC ripple, computed from the per-case values in Table IV.

Table IV compares the peak-to-peak torque ripple performance of the proposed BBFO controller and the EASMC controller under different operating conditions. The effectiveness of the BBFO controller over EASMC in reducing torque ripple across all four cases. In Case 1, BBFO achieves a ripple of 5 Nm compared to 6 Nm in EASMC, yielding a 16.67% improvement. In Case 2, BBFO reduces the ripple from 30 Nm (EASMC) to 20 Nm, achieving a 33.33% improvement. A significant enhancement is observed in Case 3, where the BBFO controller reduces the ripple by half—from 60 Nm to 30 Nm—resulting in a 50% improvement. In Case 4, BBFO lowers the ripple to 100 Nm compared to 120 Nm in EASMC, resulting in a 16.67% improvement. These results confirm that BBFO consistently outperforms EASMC, especially under higher load conditions.

TABLE IV
TORQUE RIPPLE COMPARISON: BBFO VS. EASMC

Case	BBFO (Nm)	BBFO Ripple	EASMC (Nm)	EASMC Ripple	% Improvement
Case 1	0:5	5	0:6	6	16.67%
Case 2	40:60	20	35:65	30	33.33%
Case 3	90:120	30	60:120	60	50.00%
Case 4	150:250	100	170:290	120	16.67%

Table V highlights the RMSE values in speed tracking for both BBFO and EASMC across the four operational cases. The Root Mean Square Error (RMSE) serves as a crucial metric for evaluating the precision of speed regulation. In every case, the BBFO-based controller demonstrates lower RMSE, with the highest error reduction observed in Case 1 (60%), followed by Case 3 (40%), Case 4 (33.3%), and Case 2 (28.6%). This consistent reduction underscores BBFO's superior performance in reference speed tracking. The notable accuracy of BBFO under high-speed operating conditions (2500–3000 rpm) confirms its scalability and robustness over a wide operating range.

TABLE V
SPEED TRACKING RMSE: BBFO VS. EASMC

Case	EASMC RMSE	BBFO RMSE	% Reduction
Case 1	0.05	0.02	60%
Case 2	0.07	0.05	28.6%
Case 3	0.10	0.06	40%
Case 4	0.12	0.08	33.3%

Table VI presents the comparative performance between the RTNN and the proposed BBFO control strategy for Cases 2 and 3 under loaded operating conditions. In Case 2, the proposed BBFO controller achieves superior dynamic performance with a rise time of 0.0098 s and a settling time of 0.015 s, compared with 0.0132 s and 0.024 s, respectively, for the RTNN controller. Furthermore, the RMS electromagnetic torque is reduced from 76.7 Nm for RTNN to 57.5 Nm for the proposed BBFO controller, indicating improved torque stability and smoother electromagnetic torque characteristics. Similarly, in Case 3, the proposed BBFO controller maintains better dynamic performance, with a rise time of 0.0092 s and a settling time of 0.0152 s, whereas the RTNN controller requires 0.0158 s and 0.0278 s, respectively. The RMS electromagnetic torque is further reduced from 120 Nm to 105 Nm, demonstrating the effectiveness of the proposed controller under higher load conditions. It should be noted that the values reported in Table VI correspond to the RMS electromagnetic torque, whereas Table IV presents the peak-to-peak torque ripple; therefore, the numerical values are not intended for direct comparison. Cases 1 and 4 are not included in Table VI because Case 1 represents a no-load condition with negligible performance differences, while Case 4 corresponds to an extreme load condition (200 Nm) for which comparable RTNN results are unavailable. Consequently, the comparison is limited to the representative operating conditions of Cases 2 and 3.

TABLE VI
COMPARATIVE ANALYSIS OF RMS ELECTROMAGNETIC TORQUE BETWEEN RTNN AND THE PROPOSED BBFO

Case	Control Method	Rise Time (s)	Settling Time (s)	RMS Electromagnetic Torque (Nm)
2	RTNN	0.0132	0.024	76.7
	BBFO	0.0098	0.015	57.5
3	RTNN	0.0158	0.0278	120
	BBFO	0.0092	0.0152	105

Fig. 15 presents a comparative analysis of torque ripple and speed tracking performance between the proposed BBFO controller and the existing EASMC method across four cases. The BBFO method consistently demonstrates lower torque ripple values than EASMC. For instance, in Case 1, BBFO achieves a ripple value of only 5 Nm compared to 6 Nm in EASMC, while in Case 4, the ripple is reduced to 100 Nm in BBFO against 120 Nm in EASMC.

Similarly, the top-right plot and the bottom-right bar graph illustrate the Speed Tracking RMSE values. The BBFO controller achieves significantly lower RMSE values, indicating improved speed regulation and tracking capability. For example, in Case 1, the RMSE drops to 0.02 rpm under BBFO, whereas it stands at 0.05 rpm with EASMC. In Case 4, BBFO maintains a lower RMSE of 0.08 rpm, compared to 0.12 rpm with EASMC, further emphasizing its superior dynamic response and accuracy.

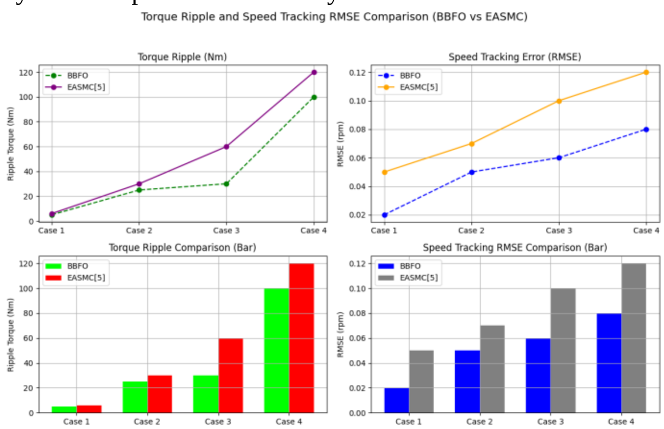

Fig. 15. Comprehensive Evaluation of Torque Ripple and Speed Tracking Performance across Cases Using BBFO and EASMC.

The bottom-left bar plot also reinforces BBFO's advantage in torque ripple mitigation. Across all cases, the green bars (BBFO) are consistently shorter than the red bars (EASMC), indicating lower ripple torque values.

To quantitatively assess the system's behaviour, the following equations were employed:

The torque ripple RMS and speed error RMSE are expressed as:

$$T_{\text{ripple, rms}} = \sqrt{\frac{1}{T}\int_0^T \left(T_{\text{actual}}(t) - T_{\text{avg}}\right)^2 dt} \tag{32}$$

$$RMSE_{\omega} = \sqrt{\frac{1}{n}\sum_{i=1}^{n}\left(\omega_{\text{ref},i} - \omega_{\text{actual},i}\right)^2} \tag{33}$$

Overall, the results demonstrate that the BBFO controller outperforms EASMC in both torque ripple reduction and speed tracking accuracy, making it a more efficient and reliable solution for the given motor control application.

V. CONCLUSION

This study presented a hybrid Bio-geography Based Firefly Optimization-based Direct Torque Control (BBFO-DTC) strategy for Switched Reluctance Motors (SRMs) to reduce torque ripple while improving speed tracking performance under varying operating conditions. The proposed controller was evaluated using MATLAB/Simulink under four operating scenarios with load torques ranging from 0 to 200 Nm and reference speeds between 1500 and 3000 rpm. The simulation results demonstrate that the proposed BBFO-DTC approach consistently outperforms the benchmark control methods. Overall, the proposed controller achieved an average torque ripple reduction of 28.2% and a maximum speed-tracking RMSE reduction of 60% compared with the benchmark controller. Furthermore, the controller maintained fast dynamic performance, with rise times ranging from 0.0083 s to 0.0111 s and settling times between 0.013 s and 0.0178 s across all operating conditions. These results indicate that the proposed BBFO-DTC strategy effectively improves torque smoothness, transient response, and speed regulation while maintaining robust performance under different load conditions.

The present study is limited to simulation-based validation using MATLAB/Simulink. Therefore, the reported performance improvements are based on simulation results, and no claims are made regarding hardware real-time implementation or processor execution capability. Nevertheless, the proposed BBFO-DTC framework provides a promising intelligent optimization strategy for enhancing SRM drive performance and offers a solid foundation for further investigation toward practical implementation.

Future work will focus on implementing the proposed controller on DSP and FPGA platforms, evaluating computational execution time and processor utilization, performing Hardware-in-the-Loop (HIL) validation, and experimentally verifying the controller using a laboratory-scale SRM prototype. In addition, future research will investigate advanced multi-objective optimization techniques to further improve power efficiency, thermal performance, and the practical feasibility of the proposed control strategy for industrial and electric vehicle applications.

Author Contributions

G. Karthikeyan. conceived the research, developed the proposed BBFO-DTC methodology, carried out the simulations, analyzed the results, and prepared the original manuscript. T. Suresh Padmanabhan supervised the research, provided technical guidance, validated the methodology, and critically reviewed and edited the manuscript. G. Jaya Bharathi contributed to the technical review, interpretation of the results, and manuscript editing. All authors read and approved the final version of the manuscript.

AI Tool Usage Acknowledgment

The authors used Grammarly to check grammar, spelling, and improve the English language and overall readability of the manuscript. The AI tool was used only for language editing and did not contribute to the research methodology, data analysis, simulation results, or scientific conclusions. The authors are fully responsible for all the content presented in this manuscript.

REFERENCES

[1] Y. Xiao, L. Shi, P. Liu, F. Han, and W. Liu, "Design of an embedded rapier loom controller and a control strategy based on SRM," IEEE Access, vol. 10, pp. 21914–21928, Feb. 2022, doi: 10.1109/ACCESS.2022.3153066.

[2] J. Sun et al., "An adaptive direct torque control with reconstructed voltage vectors for six-phase switched reluctance motor," IEEE Trans. Transport. Electrific., vol. 11, no. 2, pp. 3689–3702, Jun. 2025, doi: 10.1109/TTE.2025.3545059.

[3] O. E. Özçiflikçi and M. Koç, “Investigations of hysteresis-based direct torque controlled and field-oriented controlled IPM drives for electric vehicle applications,” J. Inst. Sci. Technol., vol. 12, no. 3, pp. 1477–1488, Sep. 2022, doi: 10.21597/jist.1132197.

[4] M. Woldeyohannes, "Analysis and model of sensor-less modified direct torque control surface permanent magnet synchronous machine for electrical submersible pumping applications," Ph.D. dissertation, Dept. Elect. Eng., Univ. South Florida, Tampa, FL, USA, 2023.

[5] G. Karthikeyan and T. S. Padmanabhan, “Enhanced adaptive sliding mode control with termination parallelism cooperative optimization for torque ripple reduction in switched reluctance motor drives,” Sci. Rep., vol. 15, Art. no. 16174, May 2025, doi: 10.1038/s41598-025-96326-7.

[6] S. E. M. Mohammadi, P. Chen, M. Moallem, B. Fahimi, and M. Kiani, “An alternate rotor geometry for switched reluctance machine with reduced torque ripple,” IEEE Trans. Energy Convers., vol. 38, no. 2, pp. 939–947, Jun. 2023, doi: 10.1109/TEC.2022.3215423.

[7] Q. Yu, X. Cao, Z. Deng, X. Deng, and C. Liu, “An improved direct displacement control for bearingless switched reluctance motors to reduce torque ripple and improve levitation performance,” IEEE Trans. Energy Convers., early access, 2024, doi: 10.1109/TEC.2024.3520777.

[8] M. R. Ashakin, B. Hossain, and S. M. H. Ifty, “Enhancing digital signal processing: Obstacles and advancements in FPGA and ASIC hardware implementations,” Pathfinder Res., vol. 2, no. 2, pp. 12–12, 2024.

[9] O. Diouri, A. Gaga, H. Ouanan, S. Senhaji, S. Faquir, and M. O. Jamil, “Comparison study of hardware architectures performance between FPGA and DSP processors for implementing digital signal processing algorithms: Application of FIR digital filter,” Results Eng., vol. 16, Art. no. 100639, Dec. 2022, doi: 10.1016/j.rineng.2022.100639.

[10] S. Chakrabarty and R. Kanagaraj, “Minimizing torque ripple for switched reluctance motor through optimum torque sharing function,” in Proc. IEEE Int. Conf. Electron., Comput. Commun. Technol. (CONNECT), Bengaluru, India, Jul. 2024, pp. 1–5, doi: 10.1109/CONNECT61668.2024.10704393.

[11] A. A. Tabassum, H. M. Cho, and M. I. Mahmud, “Essential features and torque minimization techniques for brushless direct current motor controllers in electric vehicles,” Energies, vol. 17, no. 18, Art. no. 4562, Sep. 2024, doi: 10.3390/en17184562.

[12] F. Yang, H. Chen, V. Pires, J. Martins, Y. Gorbounov, X. Li, and M. Orabi, “Improved direct torque control strategy for reducing torque ripple in switched reluctance motors,” J. Power Electron., vol. 22, no. 4, pp. 603–613, Apr. 2022, doi: 10.1007/s43236-022-00435-z.

[13] D. Samithas, P. K. Balachandran, and S. Selvarajan, “Experimental analysis of enhanced finite set model predictive control and direct torque control in SRM drives for torque ripple reduction,” Sci. Rep., vol. 14, no. 1, Art. no. 16805, Jul. 2024, doi: 10.1038/s41598-024-67554-0.

[14] Z. Niu, H. Wang, Z. Wu, J. Li, and J. Du, “Reducing torque ripples for switched reluctance motor via robust adaptive direct torque control strategy,” IEEE Trans. Power Electron., early access, 2024, doi: 10.1109/TPEL.2024.3458744.

[15] D. Mohanraj, J. Gopalakrishnan, B. Chokkalingam, and J. O. Ojo, “An enhanced model predictive direct torque control of SRM drive based on a novel modified switching strategy for low torque ripple,” IEEE J. Emerg. Sel. Topics Power Electron., vol. 12, no. 2, pp. 2203–2213, Apr. 2024, doi: 10.1109/JESTPE.2023.3297592.

[16] V. Q. Vinh and V. T. Ha, “Improved torque ripple of switched reluctance motors using sliding mode control for electric vehicles,” Eng., Technol. Appl. Sci. Res., vol. 13, no. 1, pp. 10140–10144, Feb. 2023, doi: 10.48084/etasr.5413.

[17] R. F. Soliman, M. R. Ahmed, and S. M. Sharaf, “Torque ripples reduction of switched reluctance motor using direct torque control technique,” in Proc. 25th Int. Middle East Power Syst. Conf. (MEPCON), Cairo, Egypt, Dec. 2024, pp. 1–6, doi: 10.1109/MEPCON62788.2024.10883892.

[18] M. Deepak, C. Bharatiraja, and G. Janaki, “Exploring multilevel hysteresis torque band direct torque control in switched reluctance motor drives: Insights into three and four-phase systems,” in Proc. IEEE 4th Int. Conf. Sustain. Energy Future Electr. Transp. (SEFET), Chennai, India, Jul. 2024, pp. 1–6, doi: 10.1109/SEFET61574.2024.10622808.

[19] A. Abdel-Aziz, M. Elgenedy, and B. Williams, “A new torque control approach for torque ripple minimization in switched reluctance drives,” Energies, vol. 17, no. 13, Art. no. 3334, Jul. 2024, doi: 10.3390/en17133334.

[20] M. Ghanizadeh, S. R. Mousavi-Aghdam, and M. Hoseinpour, “A modified SRM drive structure based on conventional inverter and DTC strategy to reduce torque ripple,” Energy Eng. Manag., vol. 12, no. 4, pp. 68–79, 2023.

[21] L. Al Quraan, A. L. Saleh, and L. Szamel, “Indirect instantaneous torque control for switched reluctance motor based on improved torque sharing function,” IEEE Access, vol. 12, pp. 151952–151965, Oct. 2024, doi: 10.1109/ACCESS.2024.3478015.

[22] M. L. Kimpara, R. R. Reis, L. E. da Silva, J. O. Pinto, and B. Fahimi, “A two-step control approach for torque ripple and vibration reduction in switched reluctance motor drives,” IEEE Access, vol. 10, pp. 82106–82118, Aug. 2022, doi: 10.1109/ACCESS.2022.3194885.

[23] D. Ronanki, K. R. Pittam, A. Dekka, P. Perumal, and A. R. Beig, “Phase current reconstruction method with an improved direct torque control of SRM drive for electric transportation applications,” IEEE Trans. Ind. Appl., vol. 58, no. 6, pp. 7648–7657, Nov./Dec. 2022, doi: 10.1109/TIA.2022.3205694.

[24] B. Jing, X. Dang, Z. Liu, and J. Ji, “Torque ripple suppression of switched reluctance motor with reference torque online correction,” Machines, vol. 11, no. 2, Art. no. 179, Feb. 2023, doi: 10.3390/machines11020179.

[25] B. Jing et al., “Reducing torque ripple for switched reluctance motors by current reshaping neural network,” Sci. Rep., vol. 15, Art. no. 17530, May 2025, doi: 10.1038/s41598-025-02228-z.

[26] J. Wu et al., “Direct instantaneous torque control strategy for vehicle SRM based on improved convergence rate sliding mode control,” Sci. Rep., vol. 15, Art. no. 27130, Jul. 2025, doi: 10.1038/s41598-025-06550-4.

[27] G. W. Martin, C. Agees Kumar, and J. Carol, “A modified crow search algorithm is used to minimize torque ripple for switched reluctance motor drives in electric vehicle application,” Int. J. Powertrains, vol. 14, no. 1, pp. 43–60, 2025, doi: 10.1504/IJPT.2025.146620.

[28] M. Gengaraj and L. Kalaivani, “Mitigation of torque ripple in a switched reluctance motor using an interval type II fuzzy controller,” Automatika, vol. 66, no. 4, pp. 1009–1026, 2025, doi: 10.1080/00051144.2025.2517665.

AUTHOR BIOGRAPHIES

G. Karthikeyan received the B.Tech degree in Electrical and Electronics Engineering from SASTRA, Thanjavur, Tamilnadu, India in 2008 and M.E degree in power systems engineering from Thiagarajar College of engineering, Madurai, Tamilnadu, India in 2010. He has teaching Experience of about 16 years. He is pursuing Ph.D program in Anna University, Chennai, Tamilnadu, India. He has been with the Department of Electrical and Electronics Engineering, Anjalai Ammal Engineering College, where he is currently an Assistant Professor. His research interest includes the power electronic converters for renewable energy systems, electric vehicles etc.

Dr.T.Suresh Padmanabhan was born in Nagercoil, India, in June 1980. He received a B.E degree in Electrical and Electronics Engineering from Noorul Islam College of Engineering, affiliated to Manonmaniam Sundaranar University, Tirunelveli, India, in 2001. He obtained his M.E degree in Power Electronics and Industrial Drives from Sathyabama Institute of Science and Technology, Chennai, India, in 2005. Also, he has received his Ph.D. degree in Electrical and Electronics Engineering from Pondicherry University, Pondicherry, India in 2015. Since June 2016, he has been with E.G.S. Pillay Engineering College, Nagapattiam, India. He is working as Professor in the

Electrical and Electronics Engineering department. He is having more than twenty years of teaching experience. In addition, he has authored/co-authored in several international journals and conferences. His current research interests include power electronic converters for renewable energy systems, electric vehicles, energy management systems and artificial intelligence applications in power electronic systems etc.

Mrs. G. Jaya Bharathi received the B.E degree in Electrical and Electronics Engineering from Bharathidasan University, Trichy, Tamilnadu, India in 2002 and M.E degree in power systems engineering from Anna University, Chennai, Tamilnadu, India in 2014. She has teaching Experience of about 18 years. She is pursuing Ph.D program in Anna University, Chennai, Tamilnadu, India. She has been with the department of Electrical and Electronics Engineering, Anjalai Ammal Mahalingam Engineering College, Where she is currently an Associate Professor. She is acted as nodal coordinator for value virtual labs initiative of MHRD under NMEICT. She is the Member of Indian Society for Technical Education. Her research interest includes the analysis of Energy management in micro grids, the power Electronics and Energy applications.